Available online at www.sciencedirect.com
SCIENCE DIRECT®
Agricultural and Forest Meteorology 136 (2006) 31–44
AGRICULTURAL AND FOREST METEOROLOGY
www.elsevier.com/locate/agrformet

Detection of water stress in an olive orchard with thermal remote sensing imagery

G. Sepulcre-Cantó [a], P.J. Zarco-Tejada [a,*], J.C. Jiménez-Muñoz [b], J.A. Sobrino [b], E. de Miguel [c], F.J. Villalobos [a,d]

[a] *Instituto de Agricultura Sostenible (IAS), Consejo Superior de Investigaciones Científicas (CSIC), Alameda del Obispo, s/n, 14004 Córdoba, Spain*
[b] *Universidad de Valencia, Valencia, Spain*
[c] *Laboratorio de Teledetección, Instituto Nacional de Técnica Aeroespacial (INTA), Madrid, Spain*
[d] *Dpto. de Agronomía, Universidad de Córdoba, Spain*

Received 12 May 2005; received in revised form 3 January 2006; accepted 16 January 2006

Abstract

An investigation of the detection of water stress in non-homogeneous crop canopies such as orchards using high-spatial resolution remote sensing thermal imagery is presented. An airborne campaign was conducted with the Airborne Hyperspectral Scanner (AHS) acquiring imagery in 38 spectral bands in the 0.43–12.5 μm spectral range at 2.5 m spatial resolution. The AHS sensor was flown at 7:30, 9:30 and 12:30 GMT in 25 July 2004 over an olive orchard with three different water-deficit irrigation treatments to study the spatial and diurnal variability of temperature as a function of water stress. A total of 10 AHS bands located within the thermal-infrared region were assessed for the retrieval of the land surface temperature using the *split-window* algorithm, separating pure crowns from shadows and sunlit soil pixels using the reflectance bands. Ground truth validation was conducted with infrared thermal sensors placed on top of the trees for continuous thermal data acquisition. Crown temperature (T_c), crown minus air temperature ($T_c - T_a$), and relative temperature difference to well-irrigated trees ($T_c - T_R$, where T_R is the mean temperature of the well-irrigated trees) were calculated from the ground sensors and from the AHS imagery at the crown spatial resolution. Correlation coefficients for $T_c - T_R$ between ground IRT sensors and airborne image-based AHS estimations were $R^2 = 0.50$ (7:30 GMT), $R^2 = 0.45$ (9:30 GMT) and $R^2 = 0.57$ (12:30 GMT). Relationships between leaf water potential and crown $T_c - T_a$ measured with the airborne sensor obtained determination coefficients of $R^2 = 0.62$ (7:30 GMT), $R^2 = 0.35$ (9:30 GMT) and $R^2 = 0.25$ (12:30 GMT). Images of $T_c - T_a$ and $T_c - T_R$ for the entire field were obtained at the three times during the day of the overflight, showing the spatial and temporal distribution of the thermal variability as a function of the water deficit irrigation schemes.

Keywords: Thermal remote sensing; Crown temperature; Water stress; Deficit irrigation; Split-window

1. Introduction

The estimated *Olea europaea* L. (olive trees) cultivated area in Spain is about 2,400,000 ha (AAO, 2001), with more than 200 million of olive trees. General trends for water supply limitations in Mediterranean countries make essential to understand the olive tree water relations (Orgaz and Fereres, 2004), as well as to develop measurement methods for olive tree water status and stress detection in large areas.

Canopy temperature has been suggested as a water stress indicator in several studies (Jackson et al., 1977b;

* Corresponding author. Tel.: +34 957 499 280/676 954 937; fax: +34 957 499 252.
E-mail address: pzarco@ias.csic.es (P.J. Zarco-Tejada).
URL: http://www.ias.csic.es/pzarco

0168-1923/$ – see front matter © 2006 Elsevier B.V. All rights reserved.
doi:10.1016/j.agrformet.2006.01.008

Idso et al., 1978; Jackson and Pinter, 1981). Tanner in 1963 used thermal-infrared sensors to determine the canopy temperature in potatoes, observing that temperature was a potentially reliable parameter to determine the crop water status. Other studies compared the measured canopy temperature to that of a well-watered reference plot as an indicator of water stress (Fuchs and Tanner, 1966; Clawson and Blad, 1982; Berliner et al., 1984), obtaining the relative thermal difference between well-irrigated and stressed plants. Jackson et al. (1977a) used canopy temperature (T_c) minus air temperature (T_a) as an index to study the water status of the crops, relating $T_c - T_a$ to productivity and crop water requirements. It was suggested that environmental factors like vapour pressure deficit (VPD), net radiation and wind speed could influence the canopy temperature differences. Further studies demonstrated a linear relationship between VPD and $T_c - T_a$, obtaining the crop water stress index (CWSI), which incorporated the VPD variations (Idso et al., 1981; Jackson et al., 1981). The relationship found between $T_c - T_a$ and VPD (Idso, 1982) suggested that environmental variability was an important factor, demonstrating that high values of $T_c - T_a$ were associated with water stressed plants, while low values were associated with well-irrigated plots. Moran et al. (1994) further developed the Water Deficit Index (WDI) based on $T_c - T_a$ and the Normalized Difference Vegetation Index (NDVI) to estimate the relative water status. Among other studies, these methods were then continued using infrared thermometers for stomatal conductance estimation under controlled irrigation (Jones, 1999) and using canopy temperature to estimate crop transpiration indices (Jones et al., 2002). These methods, focused on canopy temperature for monitoring stomatal conductance, are based on the effects of water stress on stomatal closure and thermal energy dissipation pathways.

Infrared technology has improved as a result of the development of light sensors with improved field of views (FOV), capable of providing greater spectral information (Wanjura et al., 2004), and enabling the monitoring of vegetation surface temperature on different spatial and temporal scales. Different sensors are currently available for the monitoring of vegetation temperature at different scales, both at airborne and satellite scales, such as the Airborne Thematic Mapper (ATM), Digital Airborne Imaging Spectrometer (DAIS), Airborne Hyperspectral Scanner (AHS), Landsat Thematic Mapper (TM), Advanced Very High Resolution Radiometer (AVHRR) and the Advanced Spaceborne Thermal Emission and Reflection Radiometer (ASTER), among others. Nevertheless, spatial and spectral characteristics of current thermal sensors onboard satellite platforms readily prevent the application of thermal detection methods for vegetation monitoring in non-homogeneous canopies, where shadow and soil background effects play an important role. Some recent studies on surface temperature estimation with high spatial resolution remote sensing imagery have proved that this technology is available for obtaining accurate measurement of surface temperature. As an example, Sobrino et al. (2004a,b) made a quality analysis of DAIS imagery comparing it with in situ surface temperature. Results showed deviations lower than 1.5 K when a vicarious calibration was conducted. It is generally accepted that the atmospheric correction and the estimation of the surface emissivity are the most important difficulties for remote sensing estimation of surface temperature Norman et al. (1995).

Various algorithms have been developed to retrieve land surface temperature from *at-sensor* and auxiliary data, such as the single-channel methods (Qin et al., 2001), *split-window* technique (Price, 1984; Becker and Li, 1990; Sobrino et al., 1991, 1994; Prata, 1993) and multi-angle methods (Prata, 1993, 1994; Sobrino et al., 1996, 2004a,b). Jiménez-Muñoz and Sobrino (2003) proposed a generalized single-channel algorithm that can be applied to different sensors onboard a satellite obtaining root mean square deviations lower than 2 K for AVHRR and ATSR-2 channel, and lower than 1.5 K for Landsat Thematic Mapper (TM). Recent studies comparing surface emissivity and radiometric temperature retrievals from the MODerate resolution Imaging Spectroradiometer (MODIS) and ASTER sensors showed good agreements, with differences lower than 0.9 K (Jacob et al., 2004). These results show high potential for remote sensing estimates of canopy temperature with medium-resolution sensors, ranging from 90 m (ASTER) to 1000 m (MODIS) pixel size. Nevertheless, there has been very limited indication in the literature showing feasible remote sensing methods for successfully linking thermal detection of vegetation and water stress in non-homogeneous tree crop canopies such as orchards. This is probably due to the requirements for using very high spatial resolution imagery (1–2 m pixel size) that enables targeting individual tree crowns and the successful separation of scene components, such as pure vegetation, soil background and shadow effects.

This study presents progress made on the application of high-spatial resolution and hyperspectral visible and near-infrared and multispectral thermal imagery, collected with the Airborne Hyperspectral Scanner, to obtain spatial and temporal variability in canopy temperature for an olive orchard under different irrigation treatments.

2. Materials and methods

2.1. Study site selection and experimental design

Research work was conducted from June to November 2004 in a 4 ha irrigated olive orchard (*Olea europaea* L. cv. 'Arbequino') located in Córdoba, southern Spain (37°48′N, 4°48′W). The climate of the area is Mediterranean with an average annual rainfall of 650 mm, concentrated from autumn to spring, and reference evapotranspiration of 1390 mm. The soils in the study area are classified as *Typic Xerofluvents* corresponding to sandy slimy soil from alluvium, with a sandy stratum at 1.5 m depth. The soil has 0.23 $m^3 m^{-3}$ high water content limit and a 0.07 $m^3 m^{-3}$ low water content limit (Testi, 2003).

The olive trees were planted in 1997 in a 3.5 m × 7.0 m pattern (408 trees ha^{-1}) with the longer dimension in the E–W direction. The olive trees were planted on ridges to avoid flooding problems. The soil was kept under no tillage using herbicides. Fig. 1 shows the study site area and the orchard field imaged by the AHS airborne sensor used in this study and described later. Three drip irrigation treatments were randomly applied within an area of six rows of 18 olive trees (2646 m^2): (i) irrigating 2.8 mm/day (well-irrigated treatment, R); (ii) 0.7 mm/day (deficit treatment, S1); and (iii) an intermittent treatment, with 1.2 mm/day from 14 June 2004 to 5 July 2004 and from 6 September 2004 to 19 October 2004, stopping irrigation from 5 July to 6 September (deficit treatment, S2) (Fig. 2).

(a)

(b)

Fig. 1. (a) Image acquired on 25 July 2004 with the Airborne Hyperspectral Scanner (AHS) sensor at 2.5 m spatial resolution, the olive grove used in this study is shown with a yellow border. (b) A close up of the olive grove. The subzone where the irrigation treatments were applied is shown with an orange border.

2.2. Field data collection

A Scholander pressure bomb (PWSC Model 3000, Soilmoisture equipment Corp., CA, USA) was used to measure leaf water potential from 11 trees covering the three irrigation treatments, measuring weekly at 10:00 Greenwich Mean Time (GMT), which is close to solar time at the longitude of our experimental site. Stomatal conductance was measured weekly every hour from 6:30 to 10:30 GMT from three trees with a leaf steady-state porometer (model PMR-4, PP Systems, Hitchin Herts, Great Britain). Leaf photosynthesis was measured weekly at 6:30, 7:30 and 10:00 GMT from six trees with a CIRAS-1 instrument (PP Systems, Hitchin Herts, Great Britain).

A total of 10 single-band infrared sensors covering the 6.5–14 μm range (model IRTS-P, Apogee, UT, USA) were placed over 10 trees comprising the three irrigation treatments in order to continuously monitor crown temperature. Previous to the field installation, the IRT sensors were calibrated in the laboratory and under natural sun conditions to characterize the IRT response to the diurnal temperature variation. Temperature over the course of the day varied between 25 and 40 °C, enabling a comparison between the IRT-estimated temperature and a thermocouple type K (chromel–alumel) in contact with the water target used for calibration. The observed errors agreed within the accuracy of the instrument (Apogee, www.apogee-inst.com) yielding a deviation of ±0.4 °C over the range of 5–40 °C range. The 52°

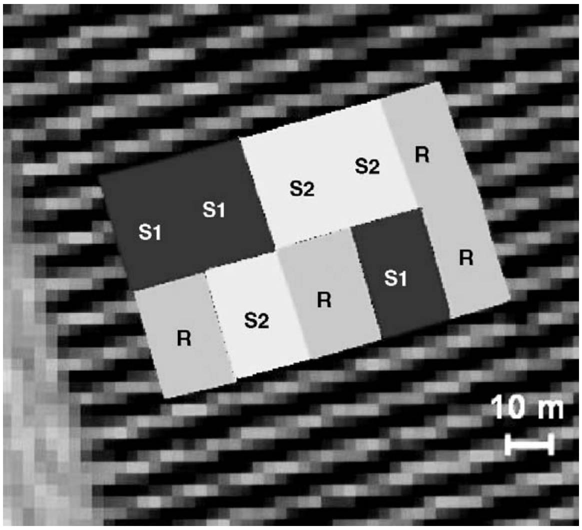

Fig. 2. An image acquired on 25 July 2004 showing the olive tree blocks under the different irrigation levels. S1 and S2 are the two deficit irrigation treatments, and R is the well-irrigated treatment. The rest of the olive orchard was drip irrigated with treatments selected in the framework of other experiments.

field of view of the IRTS-P mounted 1 m above the tree crown ensured that 85% of the signal came from the tree enabling a measurement of an integrated canopy temperature for each single tree crown (Fig. 3). A total of 300 measurements ($1\ s^{-1}$) were used to record the mean temperature at 5-min intervals in three dataloggers (model CR10X, Campbell Sci., UT, USA) placed in the study site. In addition, a field thermal radiometer Raytek (model Raynger II, Raytek, CA, USA) with a single broadband sensor covering the range 8–14 μm was used to measure temperatures over a water body. These measurements were employed to check the values retrieved from the airborne sensor data. Air temperature (T_a) data were also measured in the field at each time of image acquisition with a Vaisala Weather Transmitter (model WXT510, Vaisala Oyj, Helsinki, Finland) installed in the study plot at 1 m over a control tree (6 m above ground).

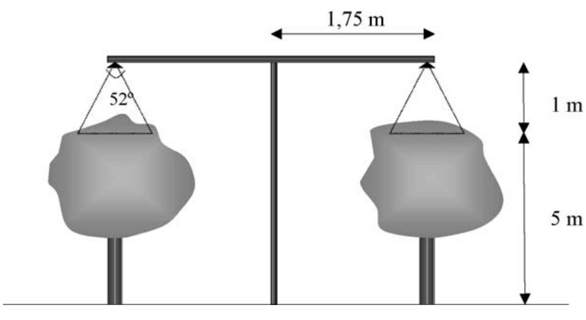

Fig. 3. Schematic view of the infrared thermal sensor installation.

2.3. Airborne campaign with the AHS sensor

The airborne campaign was conducted by the Spanish Aerospace Institute (INTA) with the Airborne Hyperspectral Scanner (developed by Sensytech Inc., currently Argon St. Inc., USA). The AHS sensor acquired imagery in 38 spectral bands in the 0.43–12.5 μm spectral range, with 90° FOV and 2.5 mrad instantaneous field of view (IFOV). The aircraft flew at 1000 m altitude above ground level (AGL), obtaining imagery at 2.5 m spatial resolution (Fig. 1). Out of the total of 10 AHS bands located within the thermal-infrared region, bands 75 (10.069 μm) and 79 (12.347 μm) were used to retrieve the land surface temperature for every pixel using the *split-window* algorithm. Spectral bands located in the visible (10 bands between 0.43 and 0.73 μm, with 0.03 μm bandwidth) and near-infrared region (10 bands between 0.73 and 1.65 μm, with 0.03 μm bandwidth) were used for pure olive-crown pixel identification and separation from soil, background targets and shadows. The airborne campaign consisted on three flights scheduled at 7:30, 9:30 and 12:30 GMT (9:30, 11:30 and 14:30 local time) on 25 July 2004, therefore enabling the study of both the diurnal and spatial variation of individual tree temperature as function of the three irrigation treatments.

2.4. Land surface temperature retrieval from AHS data: two-channel technique

Methods for land surface temperature (LST) retrieval from thermal remote sensing data are based on the radiative transfer equation applied to the thermal-infrared region (Eq. (1)).

$$L(\theta)_{\text{sensor},i} = (\theta)_{\text{surface},i}\tau(\theta)_i + L(\theta)^{\uparrow}_{\text{atm},i} \qquad (1)$$

where θ is the observation angle, τ_i the channel total transmissivity of the atmosphere in channel i, $L^{\uparrow}_{\text{atm},i}$ the upwelling atmospheric radiance in channel i and $L_{\text{surface},i}$ is the channel radiance observed in channel i at ground level (Eq. (2)).

$$L(\theta)_{\text{surface},i} = \varepsilon(\theta)_i B_i(T_s) + (1-\varepsilon(\theta)_i)L(\theta)^{\downarrow}_{\text{atm},i} \qquad (2)$$

In this equation, ε_i is the channel emissivity, $L^{\downarrow}_{\text{atm},i}$ the downwelling hemispheric atmospheric radiance in channel i and $B_i(T_s)$ is the channel radiance which would be measured if the surface were a blackbody ($\varepsilon = 1$) at temperature T_s, defined by the Planck law (Eq. (3)).

$$B_i(T_s) = \frac{C_1}{\lambda_i^5\left[\exp\left(\frac{C_2}{\lambda_i T_s}\right) - 1\right]} \tag{3}$$

with $C_1 = 1.19104 \times 10^8\ \mathrm{W\ \mu m^4\ m^{-2}\ sr^{-1}}$, $C_2 = 14387.7\ \mathrm{\mu m\ K}$ and λ_i the effective wavelength (in μm) defined as in Eq. (4):

$$\lambda_i = \frac{\int_0^\infty \lambda f_i(\lambda)\,\mathrm{d}\lambda}{\int_0^\infty f_i(\lambda)\,\mathrm{d}\lambda} \tag{4}$$

in which $f_i(\lambda)$ is the spectral response of the sensor in channel i.

A resume of methods for LST retrieval may be found in Sobrino et al. (2002, 2004a,b), Dash et al. (2002) and Kerr et al. (2004), among others. In this paper the *two-channel* technique (also called *split-window* when applied in the region 10–12.5 μm) was used. The basis of this method is that the atmospheric attenuation of the surface emitted radiance is proportional to the difference between the *at-sensor* radiances measured simultaneously in two different thermal channels (McMillin, 1975). Many papers have used this technique to extract sea surface temperature (Deschamps and Phulpin, 1980; McClain et al., 1985; Sobrino et al., 1993) and land surface temperature (Price, 1984; Becker and Li, 1990; Sobrino et al., 1991, 1994; Prata, 1993). In this study, the *two-channel* algorithm proposed by Sobrino and Raissouni (2000) and given in Eq. (5) has been used, which takes into account the emissivity and water vapour effects.

$$\begin{aligned} T_s = {} & T_i + a_1(T_i - T_j) + a_2(T_i - T_j)^2 + a_0 \\ & + (a_3 + a_4 W)(1 - \varepsilon) + (a_5 + a_6 W)\Delta\varepsilon \end{aligned} \tag{5}$$

where T_s is the surface temperature (in K), T_i and T_j the *at-sensor* brightness temperatures (K) of the thermal bands i and j, $\varepsilon = (\varepsilon_i + \varepsilon_j)/2$ and $\Delta\varepsilon = (\varepsilon_i - \varepsilon_j)$ the mean effective emissivity and the emissivity difference, W the total atmospheric water vapour (g/cm^2) and a_k ($k = 0, \ldots, 6$) are the numerical coefficients of the *two-channel* algorithm. The procedure used in order to obtain these coefficients and the results obtained with the *two-channel* algorithm are shown in Section 3.2.

3. Results and discussion

3.1. Field measurements of crown temperature and water potential

The leaf water potential responded to the water stress effects resulting from the different irrigation treatments. The leaf water potential oscillated between −0.6 and −3.3 MPa, with the lowest values corresponding to the trees under deficit irrigation treatments. Fig. 4 shows the weekly leaf water potential measurements of individual trees and the average for each irrigation treatment. Higher leaf water potential variations over the summer corresponded to trees under the greatest deficit irrigation treatment (treatment S1), with S2 (intermediate) and R (well-irrigated, Control) treatments showing differences greater than −2 MPa. The largest differences were obtained at the beginning of October, just before the onset of autumn rainfalls which caused the recovery of deficit treatments. Control trees (R) showed the leaf water potentials above −1 MPa during all the experiment. The stomatal conductance was affected due to the water stress, showing smaller values for the deficit irrigation treatments (S1 and S2). Stomatal conductance measured at 11:00 GMT varied through the experiment as a function of stress status, shifting from 8 mm s^{-1} at the time of maximum stress to 17 mm s^{-1} at recovery for treatment R, from 5 to 14 mm s^{-1}for treatment S2, and from 2 to 13 mm s^{-1} for treatment S1. The photosynthesis rate measured at 10:00 GMT showed consistently a reduction for treatment S1, throughout the experiment, yielding 10.35 μmol/m^2 s for well-irrigated trees and 6.5 μmol/m^2 s for stressed treatment S1 at the time of maximum stress (27 September 2004).

The thermal-infrared canopy temperature averaged per treatment (T_c) (Fig. 5) showed consistently that stressed trees (S1 and S2) presented higher crown temperature than well-irrigated trees (R). There were not large canopy temperature differences between treatments for either early morning and before sunrise. During midday the largest differences between treatments S1 and R for the day of the overflight (25 July 2004) were 2 K between 13:00 and 15:00 GMT (Fig. 5a and b). Larger differences were found later in the season, close to the end of the experiment, going up to 4 K temperature difference between stressed and well-irrigated olive trees (Fig. 5c and d for 23 September 2004).

Results obtained for $T_c - T_a$ for each measured tree, and for each water stress treatment for the day of the overflight (25 July 2004) are shown in Fig. 6, yielding

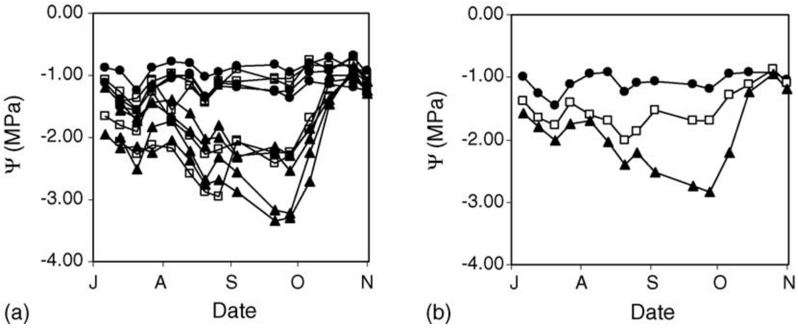

Fig. 4. (a) Weekly leaf water potential for individual trees collected between July and November 2004 and (b) averaged per treatment. S1 treatment (triangles), S2 (squares) and R (circles).

$T_c - T_a$ for the trees under treatment S1 up to 4 K at 12:00 GMT.

3.2. Airborne thermal imagery results

In order to retrieve the LST from AHS imagery using the *two-channel* algorithm given in Eq. (5), the numerical values for the coefficients a_k must be obtained using a simulation procedure and a total of 60 atmospheric profiles (the method is described in detail in Sobrino et al., 2004a,b). In this study, the radiative transfer code MODTRAN 4 and a total of 299 emissivity spectra extracted from the ASTER spectral library (http://speclib.jpl.nasa.gov) were used in the simulation procedure, versus the MODTRAN 3.5 and the eight emissivity spectra used in Sobrino et al. (2004a,b). The atmospheric region between the surface and the sensor altitude was also modified in this study, using the 1 km flight altitude of the AHS sensor and four layers in the MODTRAN code.

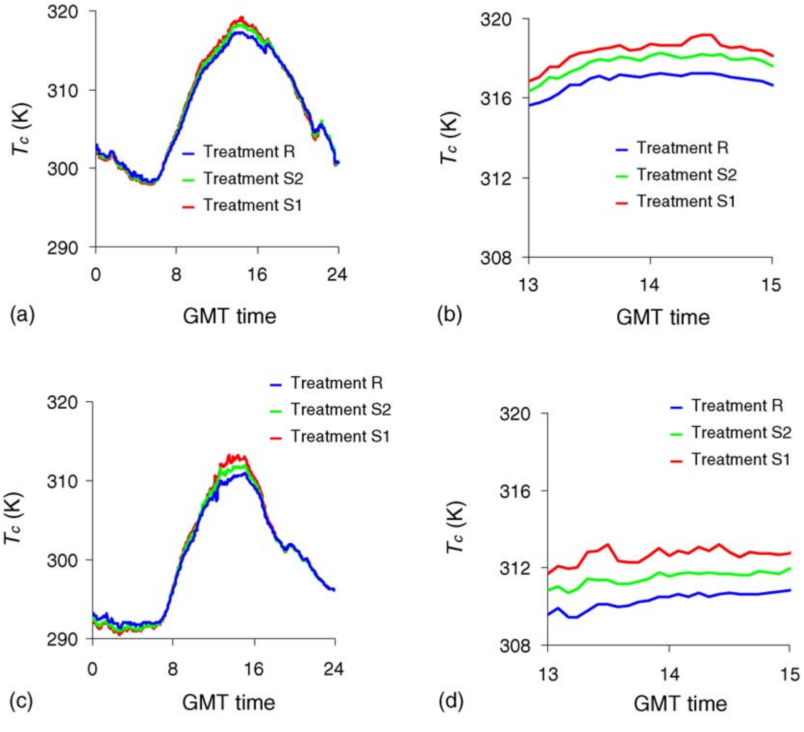

Fig. 5. (a) Diurnal canopy infrared temperature obtained per treatment on 25 July 2004, showing the data for the time period of maximum thermal differences (b). (c) Diurnal canopy infrared temperature obtained per treatment on 23 September 2004, showing the data for the time period of maximum thermal differences (d).

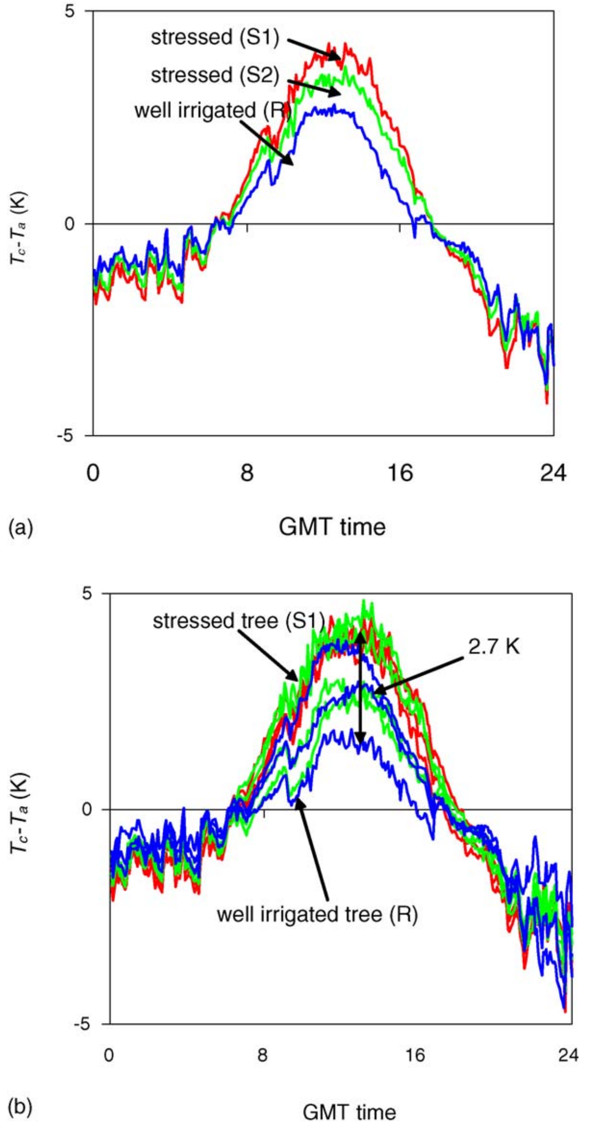

Fig. 6. (a) Diurnal infrared thermal sensor $T_c - T_a$ data (canopy temperature minus air temperature) obtained on 25 July 2004 per irrigation treatment: S1 treatment (red); S2 (green); R (blue); and (b) for individual trees.

Table 1 shows the error obtained in the sensitivity analysis for different AHS bands combinations, with bands combinations providing the worst results not shown. The sensitivity analysis has been performed following the procedure describe in Sobrino et al. (2004a,b). The results indicated that the combination between AHS band 75 (10.069 μm) and band 79 (12.347 μm) was the best choice for the LST retrieval from AHS imagery using the *split-window* algorithm, obtaining an error of 1.1 K from simulation data.

Table 1
Error in the land surface temperature retrieved with a *two-channel* algorithm (see Eq. (5)) for different Airborne Hyperspectral Scanner (AHS) band combinations

Band *i*	Band *j*	Error (K)
75 (10.07 μm)	76 (10.59 μm)	1.3
75 (10.07 μm)	77 (11.18 μm)	1.2
75 (10.07 μm)	78 (11.78 μm)	1.2
75 (10.07 μm)	79 (12.35 μm)	1.1
76 (10.59 μm)	77 (11.18 μm)	2.2
76 (10.59 μm)	78 (11.78 μm)	1.7
76 (10.59 μm)	79 (12.35 μm)	1.4
77 (11.18 μm)	78 (11.78 μm)	2.4
77 (11.18 μm)	79 (12.35 μm)	1.7
78 (11.78 μm)	79 (12.35 μm)	2.4

AHS bands 71, 72, 73, 74 and 80 not included.

Eq. (6) shows the *two-channel* algorithm with the numerical coefficients for the combination 75–79.

$$T_s = T_{75} + 0.4850(T_{75} - T_{79}) + 0.0068(T_{75} - T_{79})^2 + 0.0798 + (47.15 - 10.80W)(1 - \varepsilon) + (-49.05 + 21.53W)\Delta\varepsilon \quad (6)$$

The proposed algorithm was checked using LST values measured in situ simultaneously with the AHS flights over a water body using the field radiometer Raytek–Raynger II. Water surfaces are of great interest for validation purposes, since they are homogeneous and almost blackbodies. LST values were obtained according to Eq. (2) and by inversion of the Planck's law (Eq. (3)) using a centre wavelength of 11 μm. Downwelling atmospheric radiance was measured in the field by pointing to the sky with the radiometer, choosing a mean value for the water emissivity of 0.985. In order to apply the *split-window* algorithm given in Eq. (6), an increment in emissivity $\Delta\varepsilon = 0$ was chosen, using a value for the water vapour $W = 0.9$ g/cm^2. Water vapour was obtained by scaling to an altitude of 1 km the measured value in the 'El Arenosillo' site, part of the

Table 2
Comparison between the land surface temperature extracted from the Airborne Hyperspectral Scanner (AHS) images using the *split-window* algorithm given in Eq. (6) and the values measured in situ over a water body with the field radiometer Raytek–Raynger II

Flight (GMT)	Measured (K)	AHS (K)	AHS − measured (K)
7:30	304.8	304.2	−0.6
9:30	307.8	306.1	−1.7
12:30	308.1	307	−1.1

Bias = −1.1 K; σ = 0.6 K; RMSE = 1.3 K.

AERONET network (http://aeronet.gsfc.nasa.gov). Although this site is around 250 km away from the field site, the value was acceptable because the terms related to W in Eq. (6) are almost negligible due to the assumed high emissivity. The results obtained are shown in Table 2, with a root mean square error (RMSE) of 1.3 K. Although only three values were considered in this analysis, one per flight, results indicate that the algorithm provided good results.

In order to demonstrate that high-spatial thermal remote sensing imagery can be used to monitor diurnal thermal changes as a function of water stress conditions, three spatial levels of study were used for retrieving the plot and tree temperature from the three AHS images: (i) estimating the temperature from homogeneous treatment plots comprising 12 trees across three crop lines under the same irrigation level (Fig. 7a and d); (ii) from smaller treatment blocks comprising four contiguous trees on the

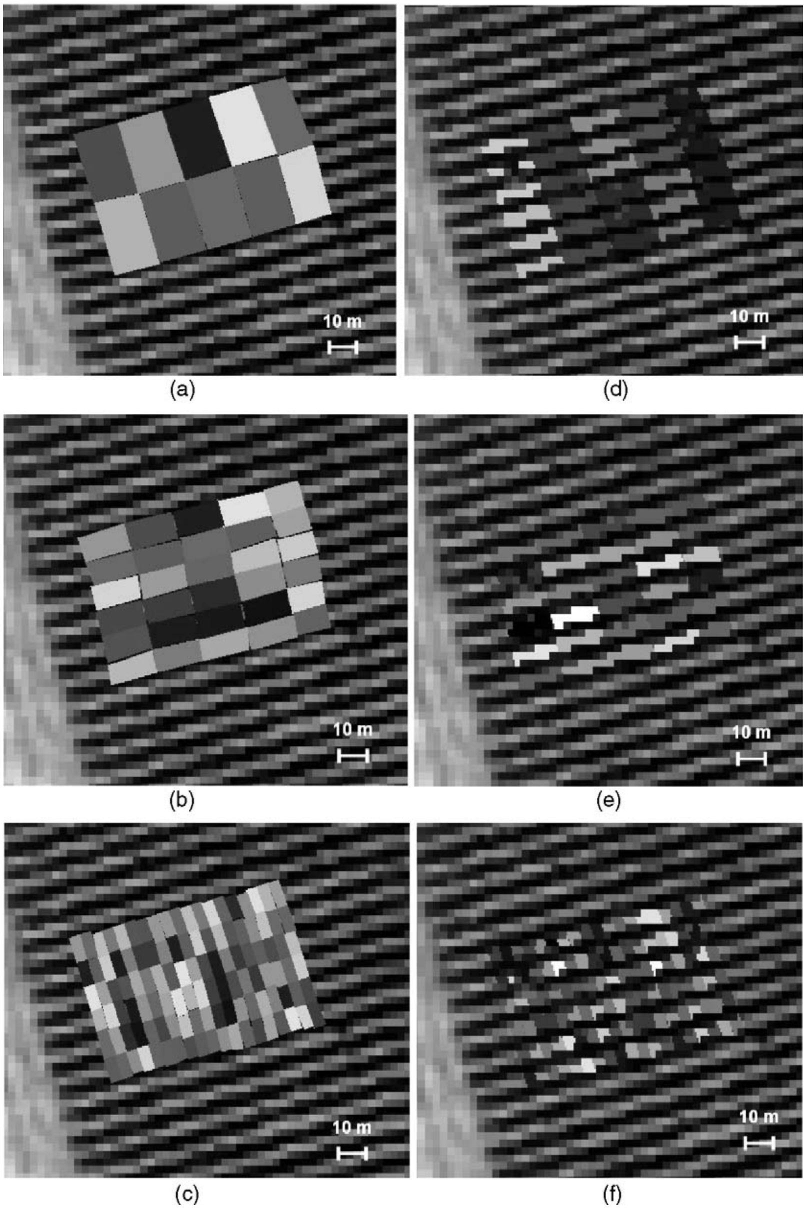

Fig. 7. Airborne Hyperspectral Scanner (AHS) images showing the blocks used for the levels of study: (a) 12 trees across three crop lines under the same irrigation level; (b) smaller treatment blocks comprising four contiguous trees along the same row; and (c) individual trees. (d–f) The thresholds applied to the imagery that enabled the identification of pure crown pixels for each level of study. The grey levels used to show the blocks under different irrigation treatments were randomly selected.

Table 3
Comparison between the land surface temperature extracted from the Airborne Hyperspectral Scanner (AHS) images using the *split-window* algorithm given in Eq. (6) and the values measured in situ with the Apogee instrument for every individual tree

Flight (GMT)	Tree	Measured (K)	AHS (K)	Measured − AHS (K)	
7:30	9–36(S2)	302.9	305.4	−2.5	Bias = −1.9 K; σ = 0.3 K; RMSE = 1.9 K
	9–37(S2)	303.2	304.8	−1.6	
	9–40(S1)	302.7	304.6	−1.9	
	9–41(S1)	302.6	304.8	−2.2	
	12–37(R)	302.6	304.2	−1.5	
	12–33(S1)	303.2	304.7	−1.5	
	12–36(R)	302.5	304.6	−2.1	
	12–44(R)	302.2	304.1	−1.9	
	12–40(S2)	302.5	304.2	−1.8	
	12–41(S2)	302.1	303.9	−1.8	
9:30	9–36(S2)	310.3	311.6	−1.3	Bias = −1.3 K; σ = 1.1 K; RMSE = 1.7 K
	9–37(S2)	310.8	311.7	−0.9	
	9–40(S1)	309.5	311.1	−1.6	
	9–41(S1)	309.4	310.7	−1.3	
	12–37(R)	309.8	310.1	−0.2	
	12–33(S1)	310.3	310.8	−0.5	
	12–36(R)	309.0	310.2	−1.2	
	12–44(R)	308.1	310.4	−2.3	
	12–40(S2)	309.0	310.7	−1.6	
	12–41(S2)	308.4	310.5	−2.1	
12:30	12–37(R)	315.5	314.7	0.9	Bias = −0.8 K; σ = 1.2 K; RMSE = 1.4 K
	12–36(R)	314.6	314.4	0.2	
	12–44(R)	313.7	314.1	−0.4	
	9–36(S2)	317.1	317.0	0.1	
	9–37(S2)	316.8	318.1	−1.3	
	12–40(S2)	314.4	314.9	−0.6	
	12–41(S2)	314.4	316.0	−1.6	
	9–40(S1)	316.2	317.9	−1.7	
	9–41(S1)	315.6	318.5	−2.9	
	12–33(S1)	316.0	317.2	−1.2	
Total bias = −1.3 K; total σ = 0.9 K; total RMSE = 1.6 K					

The notation used for the individual trees refers to the tree position in the olive orchard (irrigation treatment in brackets).

same crop line (Fig. 7b and e); and (iii) from individual trees (Fig. 7c and f). The ENVI (Research Systems Inc., USA) image processing software was used to extract image data and to calculate vegetation indices used to separate scene components. Different Normalized Difference Vegetation Index (NDVI) thresholds were applied to the imagery to successfully separate pure crowns from shadows and sunlit soil pixels, therefore enabling the estimation of the surface temperature from the pure crown component minimizing the thermal mixture of soil and shadowed soil components (Fig. 7d–f). This was of critical importance due to the large thermal differences between vegetation (tree crowns) and bare soil, yielding differences ($T_{soil} - T_c$) of up to 8 K at 7:30 GMT, 13 K at 9:30 GMT and 20 K at 12:30 GMT. The *split-window* algorithm given in Eq. (6) was applied to the three AHS images (7:30, 9:30 and 12:30 GMT) and the values for every individual tree was extracted for comparison with the in situ measurements measured by the Apogee instruments installed on the trees. Again a difference on emissivity $\Delta\varepsilon = 0$ was considered, using a mean emissivity value of 0.98 for the tree crown. This value of emissivity was obtained from the ASTER spectral library, considering tree crowns as a mixture of vegetation and trunk. Such value agrees with the emissivity of 10 trees measured in the field with the CIMEL instrument. Results shown in Table 3 indicate an RMSE of 1.6 K obtained between AHS estimated and IRT measured crown temperature. The error obtained on the LST retrieved from AHS images agrees with the expected accuracy when using thermal remote sensing data (see the references given in Section 2.4 for more details). It should be noted that the total bias obtained, 1.3 K, could be corrected from the values, obtaining in

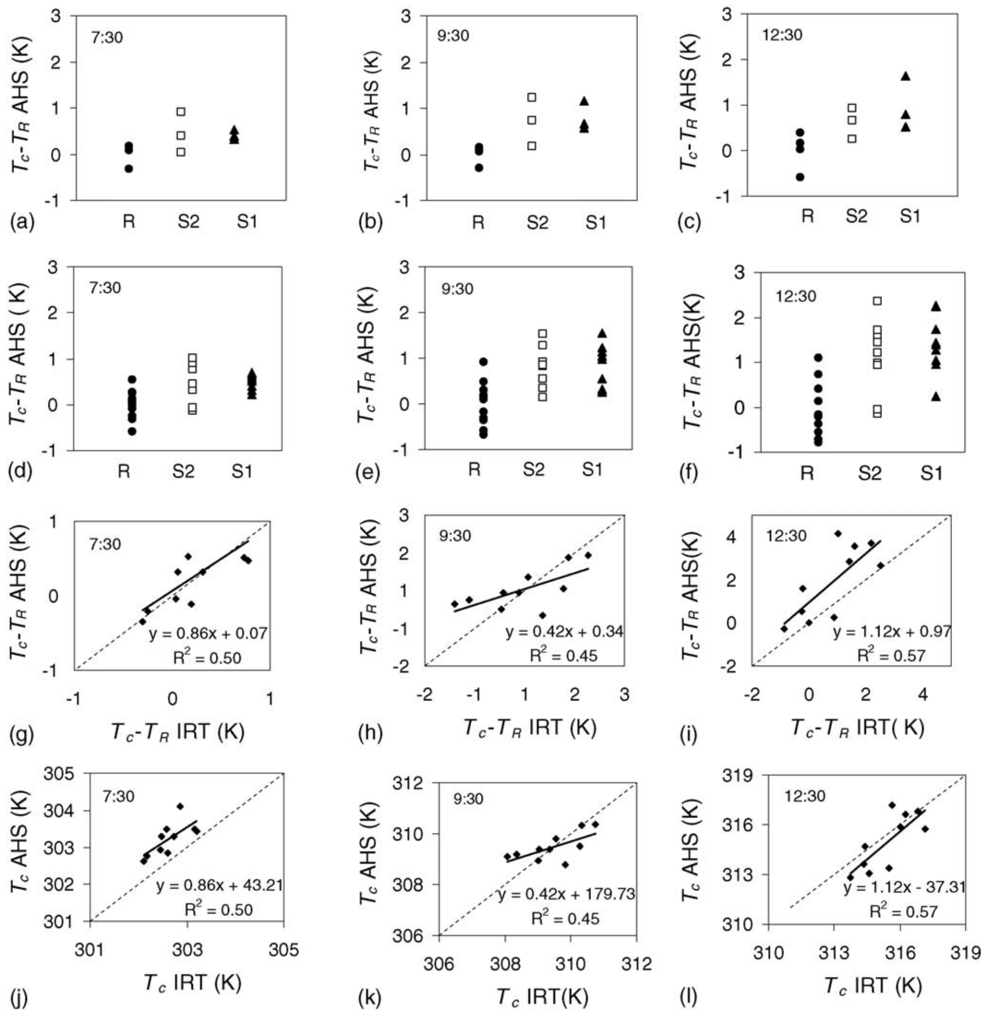

Fig. 8. Temperature differences obtained between each tree (T_c) and the mean temperature of the well-watered reference plots (T_R) from the airborne AHS sensor at the three over flight times: (a, d and g) at 7:30 GMT, (b, e and h) at 9:30 GMT and (c, f and i) at 12:30 GMT. The three levels of study were (a–c) blocks of 12 trees under the same treatment, (d–f) blocks of 4 contiguous trees on the same row and (g–i) individual trees compared with IRTS sensors placed on top of the crown. (j–l) The relationship between tree canopy temperature estimated from the AHS sensor and from the IRTS sensors at the three overflight times.

such case an error of 0.9 K, a value significantly lower than the thermal differences due to water stress.

Results obtained when comparing the thermal differences for all plots relative to those well-watered reference trees ($T_c - T_R$) estimated with the AHS sensor and for the three levels of study are shown in Fig. 8. Significant thermal differences between irrigation treatments could be identified at the three overflight times; 7:30 GMT (Fig. 8a, d and g), 9:30 GMT (Fig. 8b, e and h) and 12:30 GMT (Fig. 8c, f and i), showing higher temperature differences for S1 and S2 deficit irrigation treatments as compared with well-irrigated trees (R). These results are consistent for the three times of data collection and levels of study, with blocks comprising 12 trees across thee rows under the same irrigation level (Fig. 8a–c), and the smaller treatment blocks comprising four contiguous trees on the same row (Fig. 8d–f). The relationships found for individual trees at the time of the three overflights between ground truth IRTS and airborne AHS estimated $T_c - T_R$ (Fig. 8g–i) were $R^2 = 0.50$ (7:30 GMT), $R^2 = 0.45$ (9:30 GMT) and $R^2 = 0.57$ (12:30 GMT), suggesting that the airborne imagery was able to monitor thermal differences at the individual tree and block levels as function of the water stress. The relationships between single tree temperature obtained from the AHS airborne

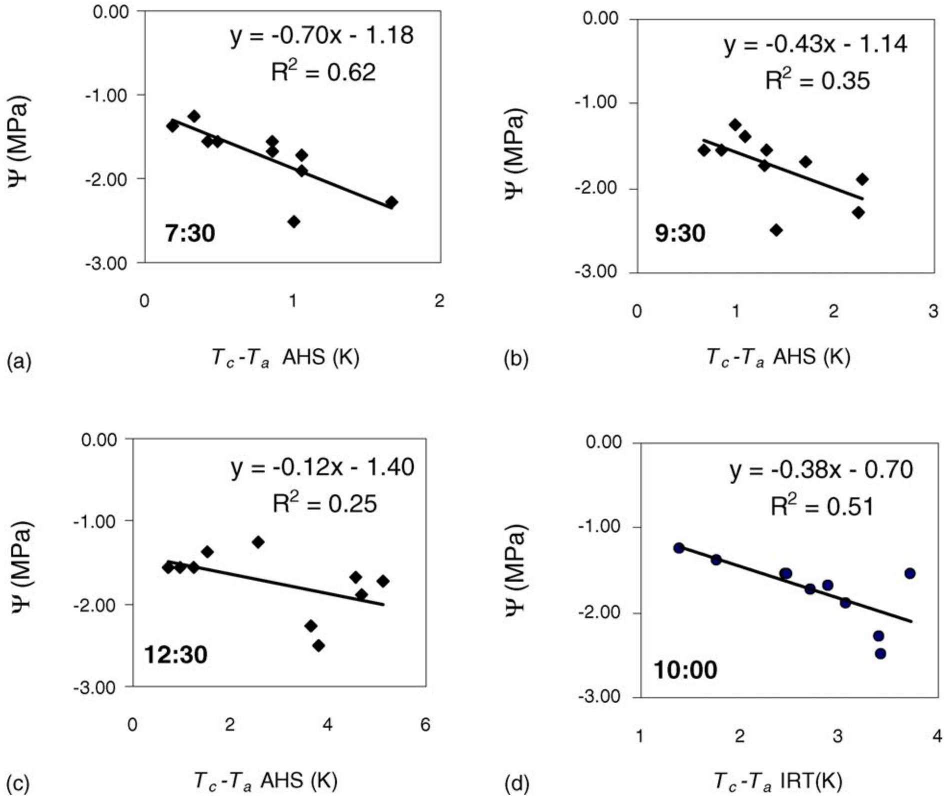

Fig. 9. (a) Relationship between leaf water potential and $T_c - T_a$ (canopy temperature minus air temperature) obtained with the Airborne Hyperspectral Scanner (AHS) imagery at 7:30 GMT, (b) at 9:30 GMT and (c) at 12:30 GMT. (d) The relationship between leaf water potential and $T_c - T_a$ obtained with the infrared thermal sensors collected in the field at 10:00 GMT.

sensor and measured in the field with the IRTS sensors at the three overflight times (Fig. 8j–l) show the capability of this method and the AHS airborne sensor to obtain the absolute temperature of individual trees.

The relationships between leaf water potential measured at 10:00 GMT on each tree, and $T_c - T_a$ estimated from the AHS imagery are shown in Fig. 9a–c for the three overflights at 7:30 ($R^2 = 0.62$), 9:30 ($R^2 = 0.35$) and 12:30 GMT ($R^2 = 0.25$). Early morning measurements provided the best results for detecting leaf water potential changes, probably due to minimal temperature differences between soil and vegetation. These results suggest that high-spatial thermal imagery is potentially capable of detecting water stress levels on individual trees as a function of canopy temperature. These results are consistent with the relationship obtained between leaf water potential and the $T_c - T_a$ data measured in the field with the field IRT sensors for each tree (Fig. 9d) yielding $R^2 = 0.51$. The consistency of these results obtained between image-estimated and ground-measured crown temperature enabled the generation of the spatial distribution of $T_c - T_R$ and $T_c - T_a$ for each airborne acquisition. The spatial distribution of the crown thermal differences relative to the well-watered reference plots for each overflight (Fig. 10a–c) shows an increasing number of trees with differences larger than 2 K relative to the reference trees. Fig. 10d–f shows the spatial distribution of $T_c - T_a$ over the course of the day, obtaining differences larger than 4 K at midday (12:30 GMT) and smaller than 1 K in the morning (7:30 GMT). The treatment blocks used for the deficit irrigation experiment part of this study are not detected in the larger scale images presented in Fig. 10, which show the spatial variability of the 1800 orchard trees. The bottom left area with a distinct feature shown was caused by a previous experiment on vegetation cover, which damaged the trees.

It should be noted that accurate LST values could also be achieved with multispectral thermal techniques, like the Temperature and Emissivity Separation (TES) method, developed by Gillespie et al. (1998), which is also capable of providing land surface emissivities. However, this method requires accurate atmospheric

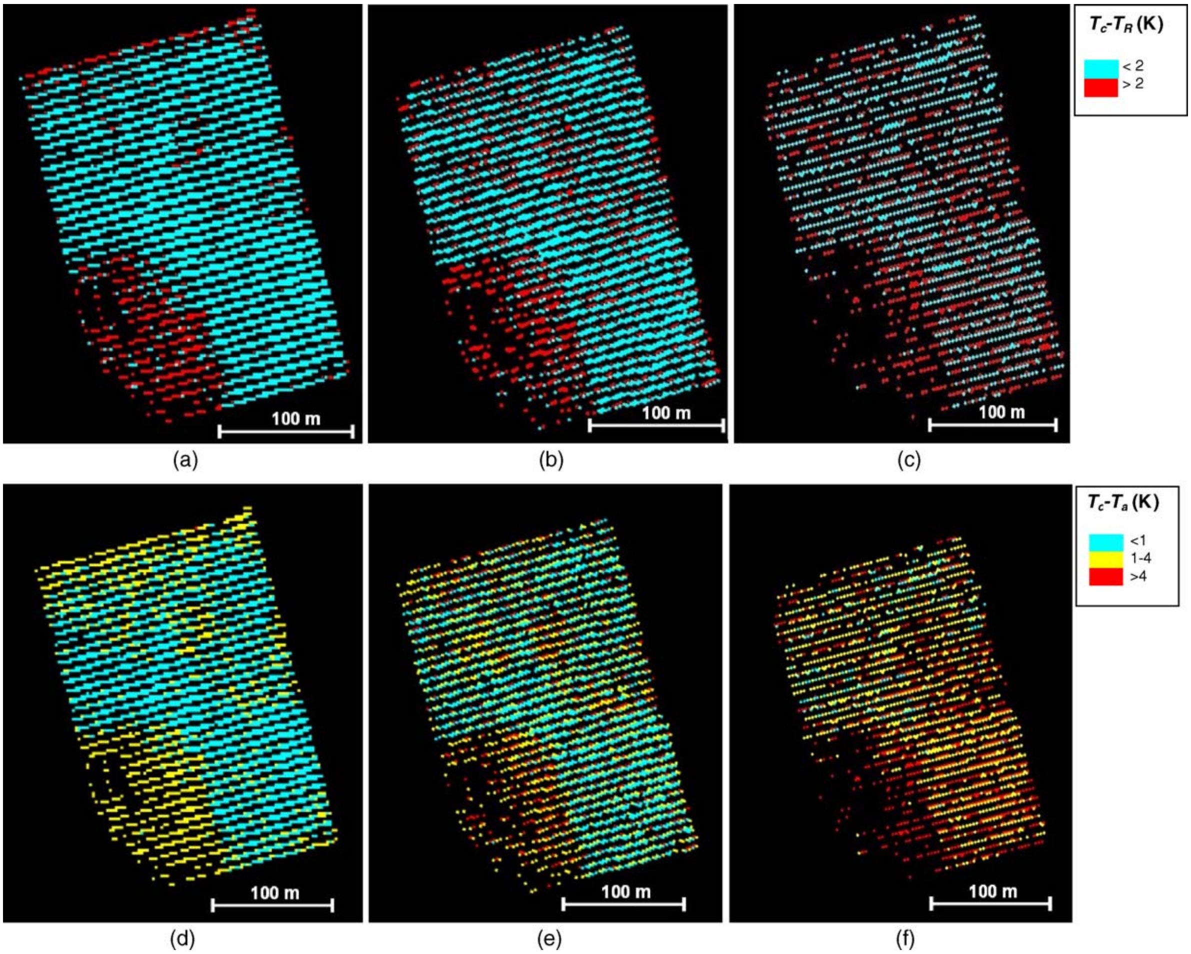

Fig. 10. (a–c) The $T_c - T_R$ (relative temperature difference compared to well-irrigated trees) images obtained with the AHS sensor on 25 July 2004 at three overflight times: (a) at 7:30 GMT, (b) at 9:30 GMT and (c) at 12:30 GMT. (d–f) The $T_c - T_a$ (canopy temperature minus air temperature) images obtained from the AHS sensor on 25 July 2004 at three over fight times: (d) at 7:30 GMT, (e) at 9:30 GMT and (f) at 12:30 GMT. The area represented is the same as that shown in Fig. 1 with a yellow border.

correction and calibration of thermal bands, which is a stricter requirement than the methodology followed herein. The application of the TES and other multispectral methods to the AHS thermal bands for both land surface temperature and emissivity retrieval is a future objective of the authors of this study.

4. Conclusions

This study makes progress on the application of thermal remote sensing methods for water stress detection in non-homogeneous orchard canopies, obtaining temperature estimates of individual tree crowns from airborne imagery. The high-spatial resolution and hyperspectral visible and near-infrared imagery and multispectral thermal data collected with the Airborne Hyperspectral Scanner enabled the study of the spatial and temporal thermal effects of water stress at the tree and orchard block irrigation levels. Leaf water potential, stomatal conductance and photosynthesis measurements in olive trees were shown to be affected during the course of the experiment using three irrigation treatments. Results obtained with the AHS airborne imager and validated with ground-truth IRTS sensors placed over the trees demonstrated that crown thermal variations associated with water stress could be detected at the tree level on the imagery, showing higher temperature differences for S1 and S2 deficit irrigation treatments as compared with well-irrigated trees (R), with differences of up to 4 K at 12:00 GMT. Relationships for the absolute crown temperature between ground IRT sensors and airborne image-based AHS estimations were $R^2 = 0.50$ (7:30 GMT), $R^2 = 0.45$ (9:30 GMT) and $R^2 = 0.57$ (12:30 GMT). The relationships obtained between leaf water potential and $T_c - T_a$ obtained from the airborne AHS imagery ($R^2 = 0.62$ at 7:30 GMT, $R^2 = 0.35$ at 9:30 GMT and $R^2 = 0.25$ at 12:30 GMT) suggest that high-spatial thermal AHS imagery is potentially capable of detecting water stress at the tree level as function of canopy temperature. The good root mean square deviation obtained for the land surface temperature retrieved from AHS data using a *split-window* algorithm, 1.6 K (or 0.9 K when the bias is corrected), indicate the feasibility for airborne-based within-field thermal variability detection at the tree level in non-homogeneous orchard crop canopies when using high-spatial resolution imagery.

The methods presented here enabled the generation of crown-level maps of $T_c - T_a$ and $T_c - T_R$ at 2.5 m spatial resolution, showing the within-field spatial and diurnal variability of the tree temperature. These methods have potential applications in water stress detection and irrigation scheduling in orchard canopies in the context of precision agriculture.

Acknowledgements

Financial support from the Spanish Ministry of Science and Technology (MCyT) for the projects AGL2002-04407-C03 and AGL2003-01468, and financial support to P.J. Zarco-Tejada from the *Ramón y Cajal* (MCyT) and *Averroes* (JA) programs are gratefully acknowledged. E. Fereres, O. Pérez-Priego, L. Testi and I. Calatrava are acknowledged for scientific and technical support. We thank J. Díaz and the INTA group for efficient airborne field campaigns providing coordination with field data collection. The UGC members M. Zaragoza, G. Soria, M. Romaguera and J. Cuenca are acknowledged for measurements and technical support in the field campaign. S. Moran and S. Ustin are acknowledged for reviewing the manuscript.

References

Agencia para el Aceite de Oliva, AAO, 2001 (www.tierra.mapya.es).

Becker, F., Li, Z., 1990. Towards a local split-window method over land surfaces. Int. J. Remote Sens. 11 (3), 369–393.

Berliner, P., Osterhuis, D.M., Green, G.C., 1984. Evaluation of the infrared thermometer as a crop stress detector. Agric. Forest Meteorol. 31, 219–230.

Clawson, K.L., Blad, B.L., 1982. Infrared thermometry for scheduling irrigation of corn. Agronomy J. 74, 311–316.

Dash, P., Göttsche, F.M., Olesen, F.S., 2002. Potential of MSG for surface temperature and emissivity estimation: considerations for real-time applications. Int. J. Remote Sens. 23 (20), 4511–4518.

Deschamps, P.Y., Phulpin, T., 1980. Atmospheric correction of infrared measurements of sea surface temperature using channels at 3.7, 11 and 12 μm. Boundary Layer Meteorol. 18, 131–143.

Fuchs, M., Tanner, C.B., 1966. Infrared thermometry of vegetation. Agronomy J. 58, 597–601.

Gillespie, A.R., Rokugawa, S., Hook, S., Matsunaga, T., Kahle, A.B., 1998. A temperature and emissivity separation algorithm for Advanced Spaceborne Thermal Emission and Reflection Radiometer (ASTER) images. IEEE Trans. Geosci. Remote Sens. 36, 1113–1126.

Idso, S.B., Jackson, R.D., Reginato, R.J., 1978. Extending the "degree day" concept of phenomenological development to include water stress effects. Ecology 59, 431–433.

Idso, S.B., Jackson, R.D., Pinter, P.J., Reginato, R.J., Hatfield, J.L., 1981. Normalizing the stress-degree-day parameter for environmental variability. Agric. Forest Meteorol. 24, 45–55.

Idso, S.B., 1982. Non-water-stressed baselines: a key to measuring and interpreting plant water stress. Agric. Meteorol. 27, 59–70.

Jackson, R.D., Pinter Jr., P.J., 1981. Detection of water stress in wheat by measurement of reflected solar and emitted thermal IR radiation. In: Spectral Signatures of Objects in Remote Sensing, Institut National de la Recherche Agronomique, Versailles, France, pp. 399–406.

Jackson, R.D., Reginato, R.J., Idso, S.B., 1977a. Wheat canopy temperature: a practical tool for evaluating water requirements. Water Resour. Res. 13, 651–656.

Jackson, R.D., Idso, S.B., Reginato, R.J., Ehrler, W.L., 1977b. Crop temperature reveals stress. Crop Soils 29, 10–13.

Jackson, R.D., Idso, S.B., Reginato, R.J., Pinter, J.R., 1981. Canopy temperature as a crop water stress indicator. Water Resour. Res. 17 (4), 1133–1138.

Jacob, F., Petitcolin, F., Schmugge, T., Vermote, E., French, A., Ogawa, K., 2004. Comparison of land surface emissivity and radiometric temperature derived from MODIS and ASTER sensors. Remote Sens. Environ. 90, 137–152.

Jiménez-Muñoz, J.C., Sobrino, J.A., 2003. A generalized single-channel method for retrieving land surface temperature from remote sensing data. J. Geophys. Res. 18 (D22), 4688.

Jones, H.G., 1999. Use of the infrared thermometry for estimation of stomatal conductance as possible aid to irrigation scheduling. Agric. Forest Meteorol. 95, 139–149.

Jones, H.G., Stoll, M., Santos, T., de Sousa, C., Chaves, M.M., Grant, O.M., 2002. Use of infrared thermography for monitoring stomatal closure in the field: application to gravepine. J. Exp. Bot. 53, 2249–2260.

Kerr, Y.H., Lagouarde, J.P., Nerry, F., Ottlé, C., 2004. Land surface temperature retrieval techniques and applications: case of AVHRR. In: Quattrochi, D.A., Luvall, J.C. (Eds.), Thermal Remote Sensing in Land Surface Processes. CRC Press, Florida, USA, pp. 33–109.

McClain, E.P., Pichel, W.G., Walton, C.C., 1985. Comparative performance of AVHRR-Based multichannel sea surface temperatures. J. Geophys. Res. 90 (11), 587–601.

McMillin, L.M., 1975. Estimation of sea surface temperature from two infrared window measurements with different absorption. J. Geophys. Res. 80, 5113–5117.

Moran, M.S., Clarke, T.R., Inoue, Y., Vida, A., 1994. Estimating crop water deficit using the relation between surface-air temperature and spectral vegetation index. Remote Sens. Environ. 46, 246–263.

Norman, J.M., Divakarla, M., Goel, N.S., 1995. Algorithms for extracting information from remote terminal—IR observations of the earth's surface. Remote Sens. Environ. 51, 157–168.

Orgaz, F., Fereres, E., 2004. In: Fereres, E. (Ed.), 1984. Viability in Adaptative Mechanisms to Water Deficits in Annual and Perennial Crop Plants, vol. 131. Bulletin Société Botanique de France. Actualités Botaniques, pp. 17–32.

Prata, A.J., 1993. Land surface temperatures derived from the AVHRR and ATSR. 1. Theory. J. Geophys. Res. 89 (16), 689–702.

Prata, A.J., 1994. Land surface temperatures derived from the advanced very high resolution radiometer and the along-track scanning radiometer. J. Geophys. Res. 99, 13025–13058.

Price, J.C., 1984. Land surface measurements from the split window channels of the NOAA 7 AVHRR data. Int. J. Remote Sens. 20, 2367–2393.

Qin, Z., Karnieli, A., Berliner, P., 2001. A monowindow algorithm for retrieving land surface temperature from Lansat TM data and its aplication to the Israel-Egypt border region. Int. J. Remote Sens. 22 (18), 3719–3746.

Sobrino, J.A., Coll, C., Caselles, V., 1991. Atmospheric correction for land surface temperature using NOAA-11 AVHRR Channels 4 and 5. Remote Sens. Environ. 38, 19–34.

Sobrino, J.A., Jiménez-Muñoz, J.C., El-Kharraz, J., Gómez, M., Romaguera, M., Sòria, G., 2004a. Single-channel and two channel methods for land surface temperature retrieval from DAIS data and its application to the Barrax site. Int. J. Remote Sens. 25, 215–230.

Sobrino, J.A., Li, Z.L., Stoll, M.P., 1993. Impact of the atmospheric transmittance and total water vapour content in the algorithms for stimating sea surface temperatures. IEEE Trans. Geosci. Remote Sens. 33, 946–952.

Sobrino, J.A., Li, Z.L., Stoll, M.P., Becker, F., 1994. Improvements in the *split-window* technique for land surface temperature determination. IEEE Trans. Geosci. Remote Sens. 32, 243–253.

Sobrino, J.A., Li, Z.L., Stoll, M.P., Becker, F., 1996. Multi-channel and multi-angle algorithms for estimating sea and land surface temperature with ATSR data. Int. J. Remote Sens. 17, 2089–2114.

Sobrino, J.A., Raissouni, N., 2000. Toward remote sensing methods for land cover dynamic monitoring application to Morocco. Int. J. Remote Sens. 20 (2), 353–366.

Sobrino, J.A., Sòria, G., Prata, A.J., 2004b. Surface temperature retrieval from Along Track Scanning Radiometer 2 data: algorithms and validation. J. Geophys. Res. 109, D11101, doi:10.1029/2003JD004212.

Sobrino, J.A., Li, Z.-L., Sòria, G., Jiménez, J.C., 2002. Land surface temperature and emissivity retrieval from remote sensing data. Recent Res. Devel. Geophysics 4, 21–44.

Tanner, C.B., 1963. Plant temperatures. Agronomy J. 55, 210–211.

Testi, L., 2003. Medida y modelización de la evaporación de Plantaciones de Olivo (*Olea europaea* L.). PhD Thesis. Universidad de Cordoba, Spain.

Wanjura, D.F., Maas, S.C., Winslow, D.R., Upchurch, D.R., 2004. Scanned and spot measured canopy temperatures of cotton and corn. Comput. Electron. Agric. 44 (1), 33–48.